Ultrasound Tracking of the Acoustically Actuated Microswimmer

Qiyang Chen, Fang-Wei Liu, Zunding Xiao, Nitin Sharma, Sung Kwon Cho and Kang Kim

Abstract— Objective: The purpose of this paper is to demonstrate the ultrasound tracking strategy for the acoustically actuated bubble-based microswimmer. Methods: The ultrasound tracking performance is evaluated by comparing the tracking results with the camera tracking. A benchtop experiment is conducted to capture the motion of two types of microswimmers by synchronized ultrasound and camera systems. A laboratory developed tracking algorithm is utilized to estimate the trajectory for both tracking methods. Results: The trajectory reconstructed from ultrasound tracking method compares well with the conventional camera tracking, exhibiting a high accuracy and robustness for three different types of moving trajectories. Conclusion: Ultrasound tracking is an accurate and reliable approach to track the motion of the acoustically actuated microswimmers. Significance: Ultrasound imaging is a promising candidate for noninvasively tracking the motion microswimmers inside body in biomedical applications and may further promote the real-time control strategy for the microswimmers.

Index Terms—microswimmer, acoustically actuated, ultrasound tracking, biomedical applications

I. INTRODUCTION

Artificial microswimmers that can be propelled to navigate in hard-to-reach spaces and microfluidic environments inside human bodies have drawn increasing research interest over the past decades[1]–[4]. The microswimmers hold a great potential in various biomedical applications, including targeted drug delivery[5]–[8], microsurgery[8]–[11], particle separation and assembly[12]–[14], bio-sensing[8], and further promote a revolution in medicine in the future[4], [15], [16].

Manuscript submitted October 1, 2018; revised January 17, 2019; accepted February 26, 2019. This work was supported by the U.S. National Science Foundation under ECCS-1637815.

Qiyang Chen, Nitin Sharma, and Kang Kim are with the Department of Bioengineering, University of Pittsburgh, Pittsburgh, PA, 15261, USA.

Qiyang Chen and Kang Kim are with Center for Ultrasound Molecular Imaging and Therapeutics, Department of Medicine & Heart and Vascular Institute, University of Pittsburgh School of Medicine and University of Pittsburgh Medical Center (UPMC), Pittsburgh, PA, 15261, USA

Fang-Wei Liu, Zunding Xiao, Nitin Sharma, Sung Kwon Cho, and Kang Kim are with the Department of Mechanical Engineering and Materials Science, University of Pittsburgh, Pittsburgh, PA, 15261, USA.

Kang Kim is also with McGowan Institute of Regenerative Medicine, University of Pittsburgh and UPMC, Pittsburgh, PA, 15219, USA. (Correspondence e-mail: kangkim@upmc.edu).

Copyright (c) 2017 IEEE. Personal use of this material is permitted. However, permission to use this material for any other purposes must be obtained from the IEEE by sending an email to pubs-permissions@ieee.org

Whereas there have been continued progress in designing and fabricating novel microswimmers for different applications, the major challenges still remain especially when considering practical propulsion and control of the microswimmers in real biomedical environments[4], [17]. A variety of propulsion principles have been investigated, such as harness of biological[18], [19], chemical fuels[20]-[24], magnetic actuation[25]–[29]. However, they all have some limitations in practical applications. Harness of biological requires controlled environment for the bacteria to survive, which is challenging for in vivo applications. Chemical fuels are commonly not biocompatible and may do harm to human body. Magnetic actuation attracted more interest among these mechanisms. However, the actuation in general requires a set of several bulky external coils to generate a strong magnetic field and the magnetic field is not compatible with some implanted devices. Acoustic actuation is promising and appealing in real biomedical environments, since it is noninvasive and biocompatible[30]-[32]. Acoustic waves can travel through biological tissues to perform wireless actuations on microswimmers. Moreover, it would be a convenient and economic approach if translating into clinical practice.

The microswimmers with a cavity that propel by acoustic actuation have already been proposed[33]. The propulsion mechanism is based on the fact that if the oscillating Reynolds number is not too small, the oscillation of the gas-liquid interface draws the surrounding liquid from the sides and ejects it in the outgoing direction. The ejected flow is responsible for propulsion generation. When a microswimmer is immersed into water, a gaseous bubble can be trapped in the cavity due to hydrophobicity of the cavity surface. The bubble oscillates periodically under the actuation of acoustic waves and forms a jet at the open end to push the microswimmer. In earlier studies, the proof-of-concept has been successfully demonstrated using micro-fabricated microswimmers by several groups [17], [33], [34]. Subsequently, it has been shown that the bubble-based microswimmer can be selectively activated by tuning the applied acoustic wave frequencies to the resonant frequencies of individual cavities and travel in viscous fluid under acoustic actuation[35]. Two dimensional steering and propulsion was also realized by adding multiple orthogonally aligned microtubes with different lengths on the body of microswimmer [36]. Moreover, a microswimmer with armored microbubbles that showed a delayed dissolution and a longer operating life was designed and fabricated[30]. Based on the bubble oscillation principle, a miniaturized endoscope

with arrays of cavities, which can adjust the imaging angles under remote acoustic actuation, has been designed and tested in vivo[37].

For eventual translation of the microswimmer technology into biomedical applications, it is essential to build a robust tracking strategy available for in situ applications in order to locate the microswimmers and provide feedback for accurate control. There has been a lack of studies that focus on developing appropriate tracking strategies for biomedical applications of the microswimmers. Most of the studies use a camera to record the motion of microswimmers[17], [35], [36]. However, optical imaging is not accessible when the microswimmers are injected into human body due to its short imaging depth in tissues. Thus, we developed an ultrasound tracking strategy for the acoustically actuated microswimmers. Based on the design of the microswimmer, high ultrasound contrast can be provided, especially from the cavity with gaseous bubbles encapsulated, providing a strong acoustic impedance mismatch. Ultrasound imaging overall is advantageous with relatively high spatial and temporal resolution, deep accessibility, as well as safety and low cost[3]. It is also compatible with the acoustic actuation method, which is appealing for combining the propulsion and tracking sequence using the same acoustic source in the future. Thus, ultrasound is an adequate candidate for tracking the motion of the microswimmers inside body for in situ biomedical applications.

In this paper, we evaluate the ultrasound tracking of a microswimmer for the first time to the best of our knowledge by comparing with the synchronously operated camera tracking in benchtop experiments. A laboratory developed tracking algorithm is used to estimate the moving trajectory of the microswimmer captured by both imaging approaches of ultrasound and camera for comparison. The tracking performance is evaluated on a few typical moving trajectories including straight, instantaneous change in direction, and continuous change in direction like a circular motion that are realized by two different microswimmer designs.

II. METHOD

A. Fabrication and design of the microswimmers

Acoustic wave induces oscillation of a gaseous bubble and this oscillating motion in fluid generates force when the bubble is confined in a one-end-open tube. The back-and-forth motion of the gas-liquid interface results in a non-zero time-averaged flow field around the outlet of the tube, which is known as microstreaming. Microstreaming flow is able to propel objects in the direction opposite to the tube's opening, and its magnitude is mainly determined by the frequency and amplitude of the applied acoustic wave. For the bubble trapped in a tube, the amplitude of the oscillating interface reaches its maximum at resonance frequency, which depends on the dimension of the bubble. By adopting this principle, a microswimmer is fabricated by Nanoscribe Photonic Professional system (GT, Germany), a 3D laser printer utilizing two-photon polymerization. By creating hollow

microtubes in the microswimmer, the tubes will automatically entrap air inside themselves due to the hydrophobicity of the material when the microswimmer is being submerged in fluid. Further, tubes with different lengths can be selectively activated at their own resonance frequencies, thus manipulating the direction of the propulsion.

The following two designs of microswimmer were applied in the experiment, which perform (1) linear and (2) bidirectional motion respectively. The first one (Fig.1a) has single microtube passing through its geometric center, thus propelling the microswimmer straight along its axis. The microtube has a diameter of 100 µm and a length of 760 µm. In the opening section, the diameter is suddenly reduced to 80 μm over the length of 60 μm in order to lock the position of the air-water interface via surface tension. This ensures the consistent and desired bubble length through the whole experiment. A continuous waveform (CW) electrical signal of 13V_{pp} at 9.4 kHz is applied to the piezo-ceramic actuator for an optimal propulsion of this microswimmer. The second microswimmer (Fig.1b) has an additional microtube on each short side of the microswimmer, which is orthogonal to the one at the center. This side microtubes provide propulsion in the orthogonal direction, which enables turning the microswimmer. The bi-directional microswimmer has an 860 µm long center microtube with an 80 µm long neck and the 370 µm long side tube with 30 µm neck. A CW burst signal of 8.3 kHz, 18 Vpp is applied to the actuator to propel both two types of tubes. Due to the difference in length of the tubes, the air cavities inside oscillate with different amplitude in response to the same acoustic signal, resulting in different propulsion forces in each direction that are orthogonal to each other. As a result, the microswimmer travels in a circular trajectory.

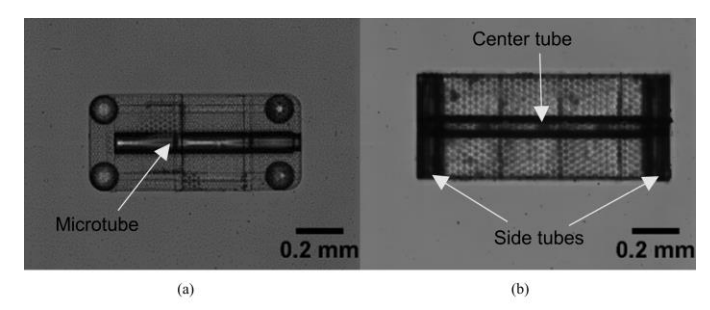


Fig. 1. (a) Microswimmer design 1 with a single microtube (100 μm in diameter and 760 μm in length). (b) Microswimmer design 2 with center (860 μm in length) and side (370 μm in length) microtubes.

B. Experiment design

The experimental setup is shown in Fig. 2. The microswimmer with single microtube is placed at the bottom of the acrylic water tank. A piezo-ceramic actuator glued to the outer surface of the water tank is utilized to generate the acoustic field that oscillates the air cavity, therefore propels the microswimmer. A CW electrical signal is generated by the function generator 1 (Agilent 33250A) through an amplifier (Trek PZD700A) to the actuator. A camera (Phantom V9.1) and two commercial ultrasound linear array transducers (L7-4,

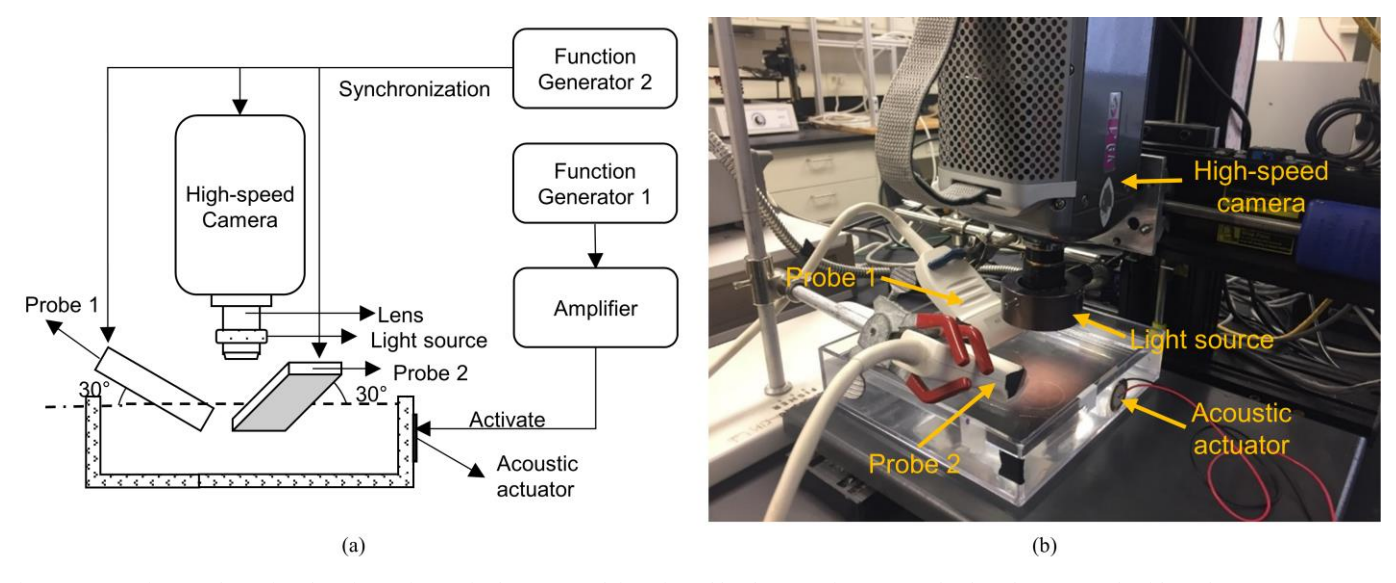


Fig. 2. (a) Experiment schematic. The microswimmer in the water tank is activated by the acoustic actuator glued on the water tank with 9.4 kHz, 13V_{pp} CW signals transmitted by function generator 1 through the amplifier. Two ultrasound linear array probes (L7-4) and a high speed camera (Phantom v9.1) are utilized to record the movement of the microswimmer simultaneously. Probe 1 and Probe 2 are connected to two separate programmable ultrasound scanners (Verasonic V1 and Verasonic Vantage, respectively). The two ultrasound probes are immersed in water at 30 degrees to the water surface. Function generator 2 is utilized to transmit TTL signals to synchronize the Phantom v9.1 camera, Probe 1 and Probe 2. (b) Experimental setup picture.

ATL) connected to a programmable ultrasound system (V1 and Vantage, Verasonics, Redmond, WA) are synchronized by the external trigger from function generator 2 (Agilent 33250A) to concurrently record the moving trajectory of the microswimmer both optically and ultrasonically. Since onedimensional (1-D) ultrasound array transducer from the top of the water surface captures only a cross-sectional image along the ultrasound beam direction (axial-lateral coordinates), two ultrasound probes are used to complement each other for capturing the full two-dimensional (2-D) motion of the microswimmer that moves along the bottom surface of the tank (x-y coordinates, see Fig. 3). Each ultrasound probe is responsible for tracking the motion along the direction of its lateral axis. Two ultrasound probes are immersed in water at 30 degrees with respect to the water surface on each side of the camera (see Fig. 2) and are positioned orthogonal to each other to provide each component of two-dimensional

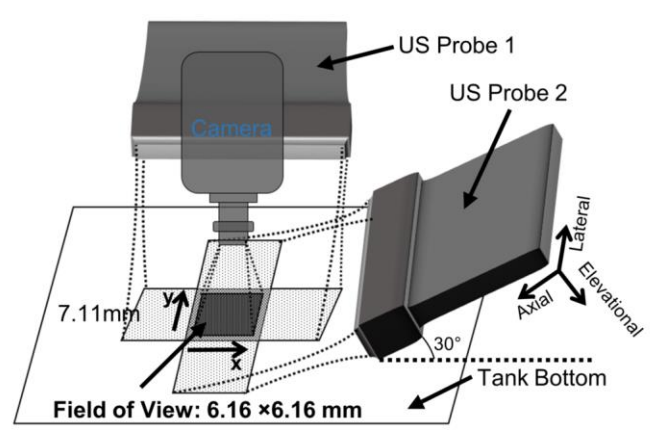


Fig. 3. Imaging field of view. The imaging field of view of each ultrasound probes is 7.11mm (elevation direction) X 36.2mm (lateral direction). The imaging field of view of the camera is 6.16 X 6.16mm with 656 X 656 pixels. The resulting imaging field of view overlaps at a 6.16 X 6.16mm area of interest.

trajectory (x-y coordinates) respectively. The intention of this unconventional placement is to avoid blocking the light source for optical imaging, and more importantly, to extend the ultrasound elevational field of view for microswimmers (see Fig. 3). The reflecting objects located within the beamwidth of the probe can be identified and reconstructed at the center line of the elevation beam by the ultrasound device [38]-[41]. By tilting the probe in elevational direction, the elevation beam area is extended so that the microswimmer moving two dimensionally at the bottom of the water tank can be tracked in a large field of view. Only the motion information along lateral axis is used because of the potential artifact along elevation axis that is attributed to the varied intensity along the elevation axis from the beam center line[38]. The elevation beamwidth projected on the motion plane of the microswimmer is measured to be 7.11mm. To align the camera field of view with the ultrasound imaging planes, a microswimmer is first placed at the center of the camera field of view. Then, the relative position of the two ultrasound probes are adjusted until ultrasound echo from the microswimmer becomes maximum. As a result, The imaging field of view of the camera and ultrasound probes are set to overlap at a 6.16 X 6.16 mm² area of interest (Fig.3). The frame rate of recording is set to 30 frames per second for both tracking methods.

C. Tracking algorithm

A tracking algorithm is developed for assessing the motion information of the microswimmer, such as displacement and direction, from which the trajectory is reconstructed. The program is written in Matlab (2017b) and applied to both ultrasound and camera video and the reconstructed trajectories from each imaging method are compared to each other. In the preconditioning procedure of the tracking algorithm, median filter is first applied to the images of all frames to minimize

4

any salt-and-pepper noise. Then, the video frames are converted to the binary images by applying a threshold. Afterwards, the microswimmer surface area is identified in the binary image and the geometrical center of the area is determined to represent the position of the microswimmer in each frame. For camera tracking, in each frame the displacement in x-y coordinates is calculated by comparing the geometrical center with that in the first frame. For ultrasound tracking, the tracking algorithm described above is applied to each ultrasound video acquired by each ultrasound

probe to estimate the geometrical center in lateral direction. The displacements in x coordinate (lateral direction of probe 1) and y coordinate (lateral direction of probe 2) are determined by comparing the geometrical centers in lateral direction with those in the first frames in two videos respectively and are then reconstructed into a complete two-dimensional x-y trajectory.

III. RESULTS AND DISCUSSION

Due to strong acoustic back scattering from the

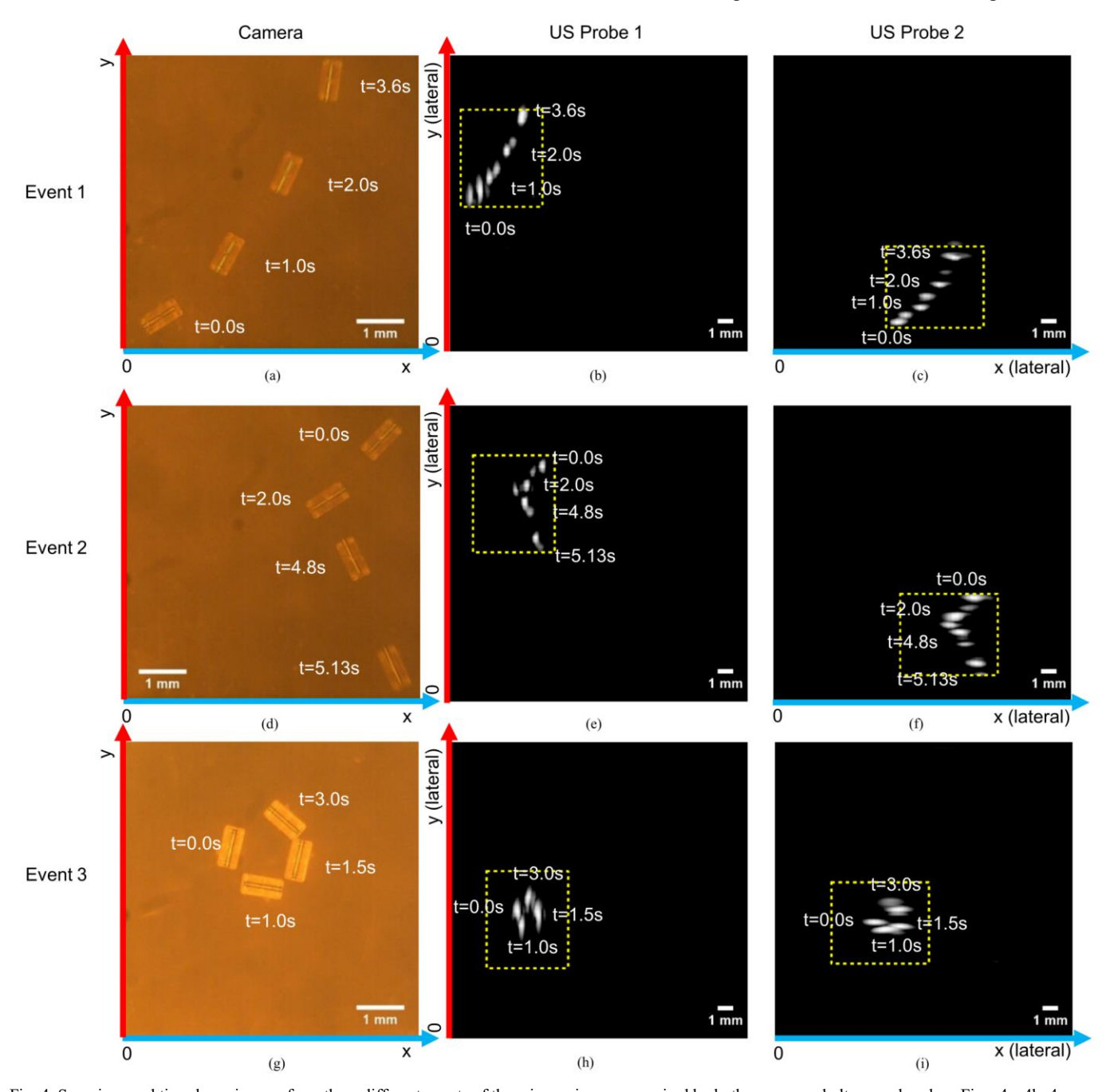


Fig. 4. Superimposed time-lapse images from three different events of the microswimmers acquired by both camera and ultrasound probes. Figs. 4a, 4b, 4c are the superimposed time-lapse images for a straight type motion of the single-tube microswimmer acquired by camera, ultrasound probe 1 and probe 2 respectively. Figs. 4d, 4e, 4f show the microswimmer motion with a sharp turn. Figs. 4g, 4h, 4i show the circular movement of the second microswimmer by camera and two ultrasound probes. The yellow dashed rectangles in Figs. 4b, 4c, 4e, 4f, 4h, 4i denote to the camera images.

microswimmer body surface and the gaseous microtube, a relatively clear image of the microswimmer with high contrast was shown by ultrasound imaging.

In Fig. 4, each row depicts the superimposed time-lapse image from each event of the microswimmer acquired by both camera and ultrasound. Event 1 and Event 2 present the movement of the single-tube microswimmer (linear motion). The single-tube microswimmer (Fig. 1a) is designed to move in a straight line under the acoustic actuation at the resonance frequency (9.4 kHz). However, due to the uneven friction at the bottom of the tank surface, the trajectory of the microswimmer slightly deviates at some location. Event 1 in Fig. 4 and supplementary video 1 taken by camera and two

ultrasound probes show that the first microswimmer (single microtube) travels straight from the lower-left corner to the upper-right corner. Event 2 in Fig. 4 and supplementary video 2 show the first microswimmer (single microtube) making a sharp turn when experiencing strong uneven friction from the bottom surface of the water tank. Event 3 in Fig. 4 and supplementary video 3 demonstrates the second microswimmer (bi-directional motion) making a circular movement. The yellow dashed rectangles in the ultrasound images denote the region of interest corresponding to camera images.

As shown in Fig. 4, a very high contrast of the microswimmer in ultrasound image allows for accurate and

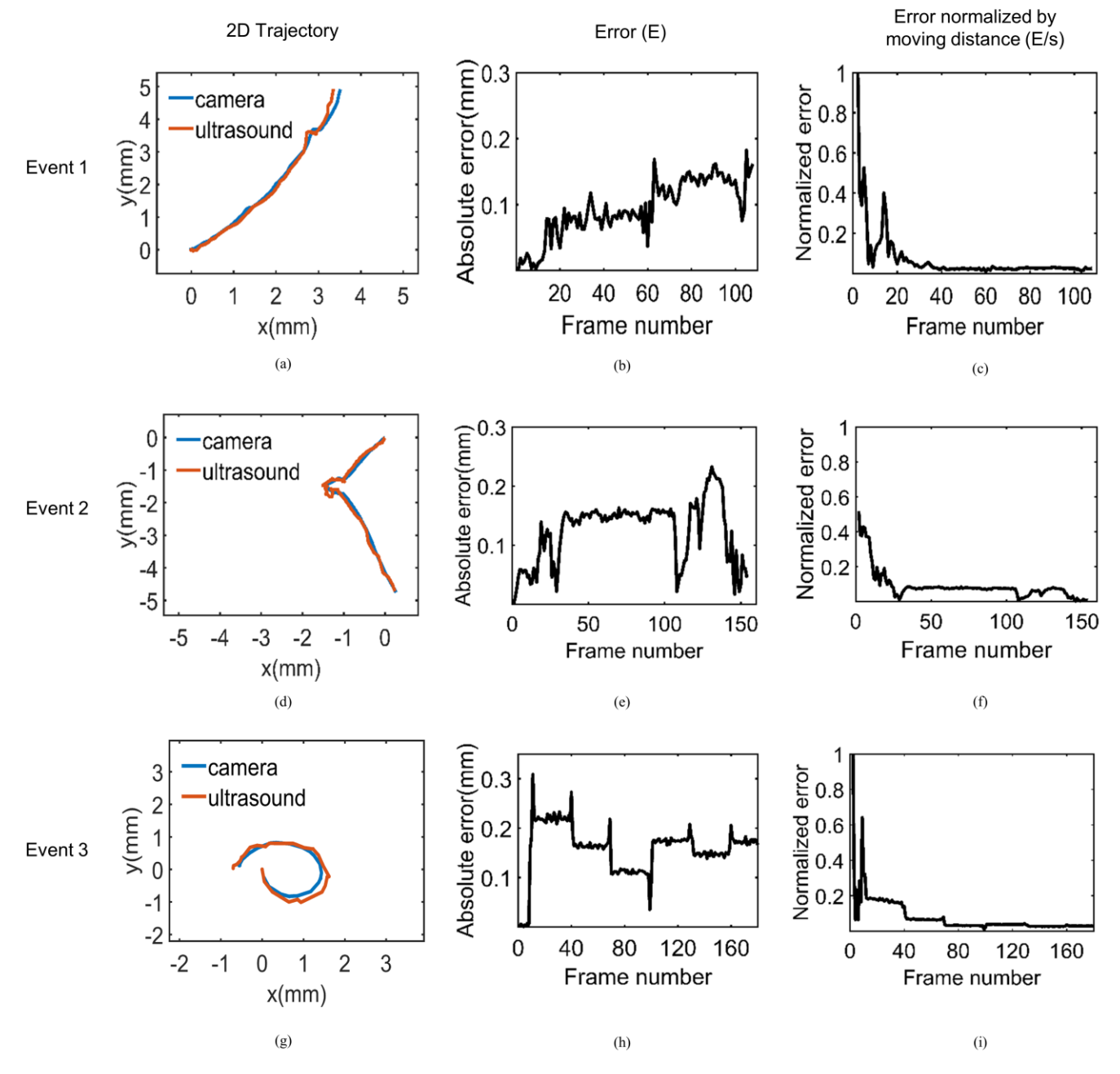


Fig. 5. Reconstructed trajectory and error analysis of ultrasound tracking for the three different events. Fig. 5a, 5d, 5g show the two-dimensional reconstructed trajectory of the microswimmer from camera and ultrasound imaging. Fig. 5b, 5e, 5h demonstrates the error (E) of ultrasound tracking compared to camera tracking (discrepancy between ultrasound and camera trajectory) at each frame. Fig. 5b, 5e, 5h show the error (E) of ultrasound tracking normalized to moving distance ($s = \sqrt{\sum_{i=0}^{t} (\Delta x)^2 + (\Delta y)^2}$) at each frame.

robust tracking. However, the appearance of the microswimmer in shape and brightness varies in the ultrasound image as the orientation of the microswimmer to the ultrasound probe changes. This is mainly attributed to the rectangular shape and nonuniform ultrasound contrast over the body of microswimmer. In one occasion, the microswimmer appears to be a single bright spot because of the strong reflection of the air cavity inside the microtube when the microtube is parallel to the lateral axis of the ultrasound probe. In other occasion when the microswimmer rotates, the single bright spot splits into two, most likely when the echoes from the two short edges of the microswimmer dominate. Thus, all the bright spots nearby within the size of microswimmer in ultrasound image are are taken and the geometrical center of them is determined as the reference point in the tracking algorithm. In this way, any potential error in locating the microswimmer caused by microswimmer body rotation can be avoided. Note that while the displacement in axial direction from the ultrasound probe can also be used to reconstruct the travel trajectory, because variation of beam intensity over the elevation axis of the ultrasound probe can be significant[38], the motion information along the axial displacement is less reliable. Thus, the lateral displacements acquire by two ultrasound probes are used to track the motion of microswimmers in this study. In Fig. 4, the lateral direction of ultrasound probe 1 and 2 are labeled in red and blue respectively, which refers to y and x coordinates in the moving plane of the microswimmer and are in accordance with the coordinates marked in the camera image.

In Fig. 5, in each row the reconstructed trajectory and the error of each event are shown. The trajectory by ultrasound tracking shown in the first column is reconstructed by the lateral displacement from each ultrasound image: lateral displacement from probe 1 corresponds to y axis; lateral displacement from probe 2 corresponds to x axis. For all three events, the trajectory by ultrasound tracking is in good agreement with the trajectory by the camera. The second column shows the error (E) of ultrasound tracking, which is defined by the discrepancy in the positions between ultrasound and camera trajectory at each frame. The error remains within ultrasound lateral resolution (~0.3 mm) except one frame in Fig. 5h, which assures that the method is reasonable and acceptable. Overall, the error of ultrasound tracking is considered mainly to be attributed to the relatively low spatial resolution of operating ultrasound frequency. Moreover, it is noted that the error becomes larger as the microswimmer rotates. This must be due to the fact that the shape of the ultrasound image of the microswimmer changes as its orientation to the ultrasound probe changes. In Fig. 5h, a few peaks indicate transiently increased errors when the microswimmer undergoes rotational motions. Due to the limited spatial resolution, ultrasound tracking is not able to identify the rotational information of the microswimmers. In addition, the tracking error can also be attributed to the relatively low signal to noise ratio especially when the microswimmer is located off the imaging center plane in the elevational direction. Column 3 shows the error (E) at each

frame normalized to the total moving distance ($s = \sqrt{\sum_{0}^{t}(\Delta x)^{2} + (\Delta y)^{2}}$) by that frame. It is noted that the error between ultrasound and camera tracking does not accumulate as the microswimmer travels. It therefore can be expected that when the microswimmer travels a quite long distance, the error of this ultrasound tracking approach stays low over the entire course of travel. In summary, the ultrasound tracking method demonstrates a good accuracy and robustness for three different types of moving trajectories in the benchtop experiments. Taking full advantage of ultrasound in general such as noninvasiveness and capability of imaging through tissues, real-time ultrasound tracking and control of the microswimmer in biomedical applications in vivo holds a promise.

There is still a room to further improve the ultrasound tracking for the acoustically-actuated microswimmers. According to the experiment results, the main limitation of this ultrasound tracking approach includes that the error can be relatively large when the microswimmer rotates, and this approach is not able to detect the angular change of the microswimmer, which is an essential information required for developing a control system for future biomedical application of the microswimmer. Applying a state estimator can be a potential approach to improve the ultrasound tracking results. The estimator corrects the ultrasound tracking results by using predictions from a dynamic model of the microswimmer. Using this estimator, accuracy of the ultrasound tracking can be improved to match the true trajectory[42]. In addition, the rotational information can be distinguished by means of optimizing the design of microswimmer. Some structures with high ultrasound contrast could be incorporated into the microswimmer to label its orientation. In the meantime, the tracking algorithm is required to be further revised and improved. Furthermore, the ultrasound tracking strategy can be combined with ultrasound actuating, and a feedback control system to promote the future clinical translation of the microswimmer technology.

IV. CONCLUSION

In this paper, we propose the ultrasound tracking strategy for the acoustically actuated bubble-based microswimmers. A benchtop experiment was conducted to compare the tracking results on three typical motion patterns acquired by synchronized camera and ultrasound tracking. The results overall indicate that ultrasound tracking is accurate and reliable to track the motion of the microswimmer. Thus, ultrasound tracking can be considered as a promising approach to track the motion of the microswimmer in biomedical applications and may further promote the real-time control strategy for the microswimmer.

REFERENCES

- [1] S. Sengupta, M. E. Ibele, and A. Sen, "Fantastic Voyage: Designing Self-Powered Nanorobots," *Angew. Chemie Int. Ed.*, vol. 51, no. 34, pp. 8434–8445, Aug. 2012.
- [2] JianFeng and S. Cho, "Mini and Micro Propulsion for Medical Swimmers," Micromachines 2014, Vol. 5, Pages 97-113, vol. 5, no.

- 1, pp. 97–113, Feb. 2014.
- [3] B. J. Nelson, I. K. Kaliakatsos, and J. J. Abbott, "Microrobots for Minimally Invasive Medicine," *Annu. Rev. Biomed. Eng.*, vol. 12, no. 1, pp. 55–85, Jul. 2010.
- [4] M. Sitti, "Miniature devices: Voyage of the microrobots," *Nature*, vol. 458, no. 7242, pp. 1121–1122, Apr. 2009.
- [5] D. Patra, S. Sengupta, W. Duan, H. Zhang, R. Pavlick, and A. Sen, "Intelligent, self-powered, drug delivery systems," *Nanoscale*, vol. 5, no. 4, pp. 1273–1283, Jan. 2013.
- [6] A. Vikram Singh and M. Sitti, "Targeted Drug Delivery and Imaging Using Mobile Milli/Microrobots: A Promising Future Towards Theranostic Pharmaceutical Design," *Curr. Pharm. Des.*, vol. 22, no. 11, pp. 1418–1428, 2016.
- [7] D. Gourevich et al., "Ultrasound-mediated targeted drug delivery with a novel cyclodextrin-based drug carrier by mechanical and thermal mechanisms," J. Control. Release, vol. 170, no. 3, pp. 316– 324, Sep. 2013.
- [8] L. K. E. A. Abdelmohsen, F. Peng, Y. Tu, and D. A. Wilson, "Micro- and nano-motors for biomedical applications," *J. Mater. Chem. B*, vol. 2, no. 17, pp. 2395–2408, Apr. 2014.
- [9] S. C. Lenaghan et al., "Grand Challenges in Bioengineered Nanorobotics for Cancer Therapy," *IEEE Trans. Biomed. Eng.*, vol. 60, no. 3, pp. 667–673, Mar. 2013.
- [10] T. Mirkovic, N. S. Zacharia, G. D. Scholes, and G. A. Ozin, "Fuel for Thought: Chemically Powered Nanomotors Out-Swim Nature's Flagellated Bacteria," ACS Nano, vol. 4, no. 4, pp. 1782–1789, Apr. 2010.
- [11] C. Bergeles and Guang-Zhong Yang, "From Passive Tool Holders to Microsurgeons: Safer, Smaller, Smarter Surgical Robots," *IEEE Trans. Biomed. Eng.*, vol. 61, no. 5, pp. 1565–1576, May 2014.
- [12] W. Yang, V. R. Misko, K. Nelissen, M. Kong, and F. M. Peeters, "Using self-driven microswimmers for particle separation," *Soft Matter*, vol. 8, no. 19, p. 5175, 2012.
- [13] N. Chronis and L. P. Lee, "Electrothermally activated SU-8 microgripper for single cell manipulation in solution," *J. Microelectromechanical Syst.*, vol. 14, no. 4, pp. 857–863, Aug. 2005.
- [14] S. Sacanna *et al.*, "Shaping colloids for self-assembly," *Nat. Commun.*, vol. 4, no. 1, p. 1688, Dec. 2013.
- [15] G. Vince and C. Wilson, "The rise of the miniature medical robots," *New Sci.*, vol. 204, no. 2735, pp. 50–53, Nov. 2009.
- [16] J. Wang, "Can Man-Made Nanomachines Compete with Nature Biomotors?," ACS Nano, vol. 3, no. 1, pp. 4–9, Jan. 2009.
- [17] J. Feng, J. Yuan, and S. K. Cho, "Micropropulsion by an Acoustic Bubble for navigating microfluidic spaces," *Lab Chip*, vol. 15, pp. 1554–1562, 2015.
- [18] S. Martel, C. C. Tremblay, S. Ngakeng, and G. Langlois, "Controlled manipulation and actuation of micro-objects with magnetotactic bacteria," *Appl. Phys. Lett.*, vol. 89, no. 23, p. 233904, Dec. 2006.
- [19] B. Behkam and M. Sitti, "Bacterial flagella-based propulsion and on/off motion control of microscale objects," *Appl. Phys. Lett.*, vol. 90, no. 2, p. 023902, Jan. 2007.
- [20] J. Simmchen, J. Katuri, W. E. Uspal, M. N. Popescu, M. Tasinkevych, and S. Sánchez, "Topographical pathways guide chemical microswimmers," *Nat. Commun.*, vol. 7, p. 10598, Feb. 2016.
- [21] W. F. Paxton et al., "Catalytic Nanomotors: Autonomous Movement of Striped Nanorods," J. Am. Chem. Soc., vol. 126, no. 41, pp. 13424–13431, Oct. 2004.
- [22] S. Ramakrishnan and C. Shannon, "Display of Solid-State Materials Using Bipolar Electrochemistry," *Langmuir*, vol. 26, no. 7, pp. 4602–4606, Apr. 2010.
- [23] G. Zhao, M. Viehrig, and M. Pumera, "Challenges of the movement of catalytic micromotors in blood," *Lab Chip*, vol. 13, no. 10, p. 1930. May 2013.
- [24] L. Restrepo-Pérez, L. Soler, C. Martínez-Cisneros, S. Sánchez, and O. G. Schmidt, "Biofunctionalized self-propelled micromotors as an alternative on-chip concentrating system," *Lab Chip*, vol. 14, no. 16, pp. 2914–2917, Jul. 2014.
- [25] R. Dreyfus, J. Baudry, M. L. Roper, M. Fermigier, H. A. Stone, and J. Bibette, "Microscopic artificial swimmers," *Nature*, vol. 437, no. 7060, pp. 862–865, Oct. 2005.
- [26] A. Snezhko, M. Belkin, I. S. Aranson, and W.-K. Kwok, "Self-Assembled Magnetic Surface Swimmers," Phys. Rev. Lett., vol.

- 102, no. 11, p. 118103, Mar. 2009.
- [27] L. Zhang et al., "Characterizing the Swimming Properties of Artificial Bacterial Flagella," Nano Lett., vol. 9, no. 10, pp. 3663– 3667, Oct. 2009.
- [28] A. Ghosh and P. Fischer, "Controlled Propulsion of Artificial Magnetic Nanostructured Propellers," *Nano Lett.*, vol. 9, no. 6, pp. 2243–2245, Jun. 2009.
- [29] R. S. M. Rikken, R. J. M. Nolte, J. C. Maan, J. C. M. van Hest, D. A. Wilson, and P. C. M. Christianen, "Manipulation of micro- and nanostructure motion with magnetic fields," *Soft Matter*, vol. 10, no. 9, pp. 1295–1308, Feb. 2014.
- [30] N. Bertin *et al.*, "Propulsion of bubble-based acoustic microswimmers," *Phys. Rev. Appl.*, vol. 4, no. 6, pp. 1–5, 2015.
- [31] M. Kaynak, A. Ozcelik, A. Nourhani, P. E. Lammert, V. H. Crespi, and T. J. Huang, "Acoustic actuation of bioinspired microswimmers," *Lab Chip*, vol. 17, no. 3, pp. 395–400, 2017.
- [32] K. J. Rao, F. Li, L. Meng, H. Zheng, F. Cai, and W. Wang, "A Force to Be Reckoned With: A Review of Synthetic Microswimmers Powered by Ultrasound," *Small*, vol. 11, no. 24, pp. 2836–2846, Jun. 2015.
- [33] R. J. Dijkink, J. P. van der Dennen, C. D. Ohl, and A. Prosperetti, "The 'acoustic scallop': a bubble-powered actuator," *J. Micromechanics Microengineering*, vol. 16, no. 8, pp. 1653–1659, 2006.
- [34] D. Ahmed, X. Mao, J. Shi, B. K. Juluri, and T. J. Huang, "A millisecond micromixer via single-bubble-based acoustic streaming †." 2009.
- [35] D. Ahmed et al., "Selectively manipulable acoustic-powered microswimmers," Sci. Rep., vol. 5, no. 1, p. 9744, Sep. 2015.
- [36] J. Feng, J. Yuan, and S. K. Cho, "2-D steering and propelling of acoustic bubble-powered microswimmers," *Lab Chip*, vol. 16, no. 12, pp. 2317–2325, 2016.
- [37] T. Qiu et al., "Wireless Acoustic-Surface Actuators for Miniaturized Endoscopes," ACS Appl. Mater. Interfaces, vol. 9, no. 49, pp. 42536–42543, Dec. 2017.
- [38] A. Goldstein and B. L, "Slice-Thickness Artif acts," *J. Clin. Ultrasound*, no. September, pp. 365–375, 1981.
- [39] M. L. Skolnick, "Estimation of ultrasound beam width in the elevation (section thickness) plane.," *Radiology*, vol. 180, no. 1, pp. 286–288, Jul. 1991.
- [40] B. Richard, "Test Object for Measurement of Section Thickness at US," *Radiology*, vol. 211, no. 1, pp. 279–282, Apr. 1999.
- [41] M. Peikari, T. K. Chen, A. Lasso, T. Heffter, and G. Fichtinger, "Effects of Ultrasound Section-Thickness on Brachytherapy Needle Tip Localization Error," Springer, Berlin, Heidelberg, 2011, pp. 299–306.
- [42] N. Sharma and A. Dani, "Nonlinear estimation of gait kinematics during functional electrical stimulation and orthosis-based walking," in 2014 American Control Conference, 2014, pp. 4778–4783.